

Trapped-Particle-Mediated Collisional Damping of Nonaxisymmetric Plasma Waves

A. A. Kabantsev and C. F. Driscoll

Department of Physics, University of California at San Diego, La Jolla, California 92093, USA

(Received 1 June 2006; published 29 August 2006)

Weak axial variations in magnetic or electric confinement fields in pure electron plasmas cause slow electrons to be trapped locally, and collisional diffusion across the trapping separatrix then causes surprisingly large trapped-particle-mediated (TPM) damping and transport effects. Here we characterize TPM damping of $m_\theta \neq 0$, $m_z = \pm 1$ Trivelpiece-Gould plasma modes in large-amplitude long-lived Bernstein-Greene-Kruskal states. The TPM damping gives $\gamma_{\text{BGK}}/\omega \sim 10^{-4}$ and seems to dominate in regimes of weak interparticle collisions.

DOI: [10.1103/PhysRevLett.97.095001](https://doi.org/10.1103/PhysRevLett.97.095001)

PACS numbers: 52.35.Fp

Theorists generally prefer Galilean invariance and Maxwellian velocity distributions, but nature often does not. In typical pure electron plasma columns, the magnetic field is axially “invariant” to within 1 part in 10^3 ; but the slow electrons trapped in the weak ripples may have near-discontinuous velocity distributions and, apparently, do cause dominant damping and transport effects. These trapped-particle-mediated (TPM) effects arise from both magnetic and electric ripples and have been observed to cause new modes [1], damping of drift modes [2], cross-field transport of particles [2–4], as well as the damping of electron plasma waves discussed here. TPM effects may dominate when collision rates ν are small compared to wave frequencies ω , since TPM effects are predicted to scale as $(\nu/\omega)^{1/2}$ rather than $(\nu/\omega)^1$.

Of course, magnetic and electric trapping is commonplace in neutral plasma physics. In toroidal geometry, the enhanced inboard magnetic field strongly constrains the poloidal rotation and gives rise to a variety of trapped-particle modes and induced currents. An incisive boundary layer analysis of the trapping separatrix predicted near-discontinuous distribution functions, with damping effects scaling as $(\nu/\omega)^{1/2}$ [5]. Later experimental work verified some aspects of trapped-particle modes (but not the damping) [6,7], and subsequent theory work has ranged from $(\nu/\omega)^{1/2}$ trapping subtleties [8] to Galilean invariance sureties [9]. A variety of TPM effects are thought to arise from helical ripples in stellarator magnetic fields [10], but experimental tests are difficult.

In contrast, theory and experiment are in general accord on a variety of *wave-trapping* effects. Particles moving near the wave phase velocity can be trapped in the wave potential, giving a localized flattening of the (presumed) Maxwellian distribution, voiding Landau damping, and enabling “steady-state” Bernstein-Greene-Kruskal (BGK) modes [11]. For electron plasma waves, the observed wave-trapping amplitude oscillations correspond closely to theory [12], and a variety of long-lived BGK states have been observed, including many with nonlinear fre-

quency shifts [13,14]. Surprisingly, the requisite wave-particle correlations persist even for standing waves in finite length apparatuses, surviving 10^3 – 10^4 end reflections of oppositely moving waves. In the present experiments, the BGK state flattens the velocity distribution for a 0.5% component of electrons, over the range $0 < v < 5\bar{v}$.

Velocity-scattering collisions necessarily dissipate these BGK states. Zakharov and Karpman [15] and others [16,17] calculated repopulation of the Maxwellian distribution at the wave phase velocity, predicting damping rates $\gamma_{\text{ZK}} \propto \nu^1$.

In this Letter, we observe a stronger damping, determined to be due to TPM effects, with damping rates consistent with a $(\nu/\omega)^{1/2}$ scaling. The trapping arises from an inherent magnetic ripple with peak $\delta B_z/B_z \sim 10^{-3}$ centered under the midplane cylinder and from negative “squeeze” voltages applied to that cylinder. This TPM damping is observed only for $m_\theta \neq 0$ modes, in which $\hat{\theta}$ wave electric fields cause radial particle drifts, with consequent phase-space discontinuities at the ripple-trapping separatrix. Analogous TPM effects would be expected in neutral plasmas.

The pure electron plasma columns described here are confined in a Penning-Malmberg trap, as shown in Fig. 1. The electrons emitted from a hot tungsten source are con-

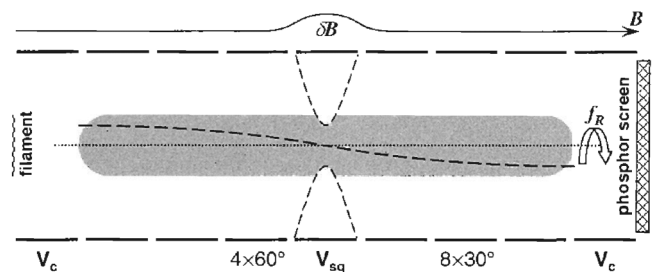


FIG. 1. Schematic of cyclinridal electron plasma with magnetic and electric ripples and an $m_z = 1$ plasma wave.

finned radially by a nearly uniform axial magnetic field $1 \leq B \leq 15$ kG and confined axially by negative voltages $V_c = -100$ V on end cylinders with radius $R_w = 3.5$ cm. Typical electron columns have density $n \sim 1.5 \times 10^7$ cm $^{-3}$ over a radius $R_p \sim 1.2$ cm and length $L_p \sim 48$ cm, giving line density $N_L \equiv \pi R_p^2 n_0 = 6.7 \times 10^7$ cm $^{-1}$. The unneutralized electron charge results in an $\mathbf{E} \times \mathbf{B}$ rotation of the column at frequency $f_R(r) = cE(r)/2\pi rB \sim (0.1 \text{ MHz})B/2 \text{ kG}^{-1}$.

The z -averaged densities $\bar{n}(r, \theta, t)$ are measured at any time by dumping the electrons axially onto a phosphor screen imaged by a CCD camera. Alternately, the z -averaged density of the right-hand end *only*, $\bar{n}_h(r, \theta, t)$, can be measured by cutting the plasma in half with $V_{sq} \sim -100$ V immediately ($0.2 \mu\text{s}$) before dumping onto the phosphor. Additionally, the distribution of axial energies $F(E_z)$ can be obtained by measuring the electrons which escape (preferentially near $r = 0$) as the end confinement V_c is slowly raised to ground (in $100 \mu\text{s}$). The initial quiescent plasmas have a thermal distribution with $T \sim 1$ eV, giving $\bar{v} \sim 42$ cm/ μs , $\lambda_D \sim 0.2$ cm, and collisional 90° scattering rate $\nu \equiv (16\sqrt{\pi}/15)n\bar{v}b^2 \ln \Lambda \sim 160 \text{ sec}^{-1}$.

Electron plasma waves in the Trivelpiece-Gould (TG) regime are excited and monitored using cylinders in each axial half incorporating $4 \times 60^\circ$ and $8 \times 30^\circ$ wall sectors, allowing unambiguous identification of the axial and azimuthal mode numbers m_z and m_θ . The modes are weakly damped standing waves in z and have the form

$$\delta n(r, \theta, z, t) = \delta n(r) \sin(m_z \pi z / L_p) \times \cos[m_\theta \theta - 2\pi f t] e^{-\gamma t}. \quad (1)$$

Here we focus on $m_z = 1$, $m_\theta = 1$, in the lowest radial mode ($m_r = 1$) with $\delta n(r) = 0$ only at $r = 0$ and $r > R_p$.

Two separate TG modes exist, either co- or counter-rotating relative to the plasma f_R . The linearized cold electron plasma dispersion relation for top-hat density profiles predicts (upper and lower) frequencies

$$f_{u,\ell} = m_\theta f_R \pm f_* \equiv m_\theta f_R \pm m_z \left(\frac{\pi R_p}{j_{m_\theta-1, m_r} L_p} \right) f_p. \quad (2)$$

The rotating-frame wave frequency scales as $f_* \propto N_L^{1/2} L_p^{-1}$, with $f_* = 1.13$ MHz for our plasmas, substantially below the plasma frequency $f_p \sim 35$ MHz. (Note that proper interpretation of theory [18] gives $j_{m_\theta-1, m_r}$ rather than j_{m_θ, m_r} .) At low amplitudes, these modes are *overdamped*, with Landau damping giving $\gamma_L \sim 2.4 f_*$, following from $v_{ph} = 2L_p f_* \sim 2.6 \bar{v}$.

Despite the strong linear damping, application of resonant oscillating wall voltages does excite either mode to a large-amplitude, long-lived BGK state. Figure 2 shows the (upper-mode) eigenfunction amplitude $\delta n(r)$ obtained immediately after excitation; the eigenfunction agrees closely with the

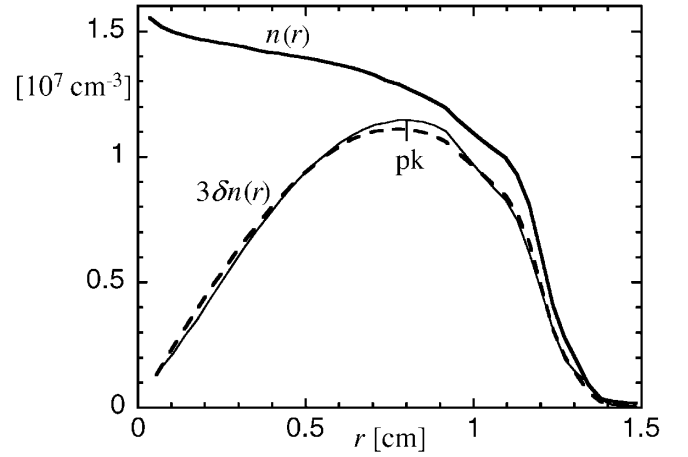


FIG. 2. Measured plasma density $n(r)$ and radial eigenfunction $\delta n(r)$ of the $m_\theta = 1$, $m_z = 1$, $m_r = 1$ plasma wave. The dashed line shows Eq. (3).

$$\delta n(r) \propto n(r) J_1(j_{0,1} r / R_p) \quad (3)$$

prediction of linear theory.

Figure 3 shows the time evolution of the mode amplitude $A \equiv (\delta n/n)_{pk}$ and frequency $f_1(t)$, obtained by fitting a local sinusoid to the waveform received on a wall sector. The $m_\theta = 1$ BGK mode damps essentially exponentially over $1 \frac{1}{2}$ decades, at a rate $\gamma_1 \sim 0.99 \times 10^3 \text{ sec}^{-1}$; this will be shown to be TPM collisional damping. At small amplitude, the wave damps much more rapidly. The mode frequency shows an ill-understood 4% decrease during excitation and the first 200 wave cycles ($200 \mu\text{sec}$) and then shows a characteristic logarithmic increase [a retreat back to $f_1(0)$] as the amplitude decreases. This latter evolution is well-approximated by $f(A) = f_0 [1 - \alpha \ln(1 + \beta A)]$. We note that the same amplitude dependence is observed with larger α for $m_\theta = 0$, $m_r = 1$ BGK

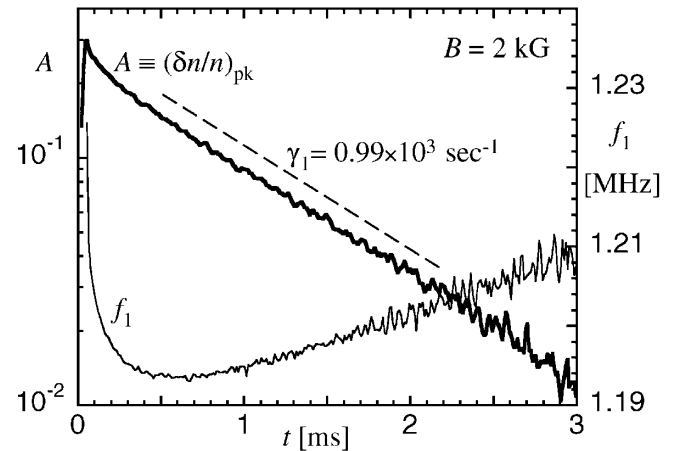


FIG. 3. Peak mode amplitude and frequency vs time after excitation.

states (apparently not mitigated by $\pm\theta$ or radial layer cancellations).

Several experimental manipulations help to characterize the BGK mode. First, the damping can be greatly and immediately enhanced ($5\text{--}10\times$) by lowering the end confinement voltage V_c , thereby allowing electrons in the wave-trapped phase-space vortex to escape. The wave then continually accelerates electrons to high velocities where they escape, and the wave damps rapidly.

This wave-trapped vortex is a “flat” component of $F(E_z)$ comprising about 0.5% of the electrons. To obtain $F(E_z)$, the number of escaping electrons ΔN_e is measured as the dump-end confinement voltage is ramped from $V_c = -100$ V to $V_c = -30$ V (close to the plasma potential ϕ_p) in a time of 100 μs , shown in Fig. 4. One expects $\Delta N_e = \int dr \int_{\phi_p(r)-V_c}^{\infty} d\varepsilon F(\varepsilon)$. Before (and long after) the wave is excited, the observed $\Delta N_e(V_c)$ is exponential, reflecting a Maxwellian tail with $T \sim 1$ eV, obtained as $\kappa e/T = d\ln(\Delta N)/dV_c$, with geometry coefficient $\kappa = 0.87 \times 1.05 = 0.9$ [19]. During the BGK wave, the $\Delta N_e(V_c)$ data reflect this Maxwellian distribution *plus* a flat distribution extending from $\varepsilon = 0$ to $\varepsilon_{\text{max}} = 17$ T, corresponding to applied voltage $V_c^{(\text{max})} = \phi_p - \varepsilon_{\text{max}}/0.87e \sim -50$ V. This maximum wave-trapping energy determines the wave potential: $\varepsilon_{\text{max}} = \frac{1}{2}m(v_{\text{ph}} + \delta v_{\text{trap}})^2 \sim 17$ T and $v_{\phi} \sim 2.6\bar{v}$ implies $\delta v_{\text{trap}} \sim 3.2\bar{v}$, giving $\delta\phi_{\text{trap}} \sim 1.8$ V = 1.8 T/e. This corresponds well to the wave potential $\delta\phi^{\text{pk}} \sim 2.4$ V obtained from the peak amplitude of Fig. 3, given that the quantitative effects of r averaging have not been calculated.

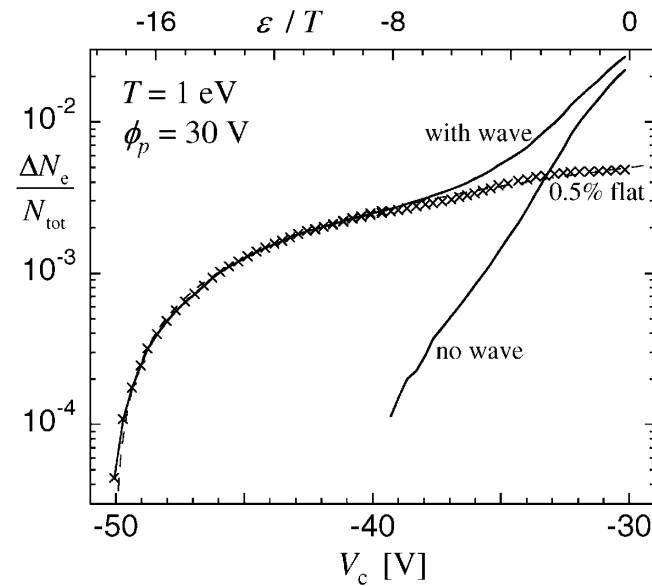


FIG. 4. Fraction of escaped electrons ΔN_e vs confinement potential V_c or thermal energy ε/T with and without wave. The measured difference (crosses) closely corresponds to a 0.5% flat fraction extending to 17 T (dashed line).

Second, the $m_\theta = 1$ BGK mode damping rate γ_1 can be enhanced by excitation of $m_\theta = 0$, $m_z = 1$, $m_r = 1$ (“sloshing”) modes of moderate amplitude, and the damping increment is observed to be proportional to the excitation amplitude. The $m_\theta = 0$ mode causes potential variations on $\pm z$ ends of the ripple-trapping barrier(s) at the midplane, resulting in enhanced ripple-separatrix crossings and enhanced $m_\theta = 1$ mode damping. This technique has been used extensively to characterize TPM mode damping and particle transport [4] and even to diagnose $F(E_z, r)$ at the separatrix velocity $v_s(r)$ [20].

Third and most incisive, the BGK state damping can be enhanced by application of near-dc squeeze voltages on the midplane cylinder: these create *electric* trapping barriers in addition to the always-present magnetic ripple-trapping barriers. Figure 5 shows the instantaneous effect on damping rate γ_1 from a positive or negative ramped squeeze voltage applied to the midplane cylinder. Note that this is coincident axially with the predominant magnetic ripple (mirror) of $\delta B/B \sim 10^{-3}$ and with the node of the standing plasma wave. The positive squeeze has little effect, whereas the negative voltage creates an electric trapping barrier which gives strong TPM damping from the electric trapping barrier.

We interpret the observed damping as due to separate electric and magnetic trapping barriers, i.e., $\gamma_1 = \gamma_E + \gamma_M$. The electric-TPM component γ_E is proportional to the strength of the electric trapping barrier, as shown in Fig. 6. Here the instantaneous damping rate γ_1 is plotted versus the instantaneous (negative) squeeze voltage V_{sq} for 4 different plasmas at varying temperatures. For $V_{\text{sq}} = 0$, a (more accurate) damping rate is obtained over longer times, and this is interpreted as γ_M due to the inherent magnetic ripple. Prior experiments on cross-field transport and diocotron mode damping clearly isolated the magnetic ripple effects [2–4]; here the requirement of 2 sectorized cylinders precludes removal of the ripple. The different

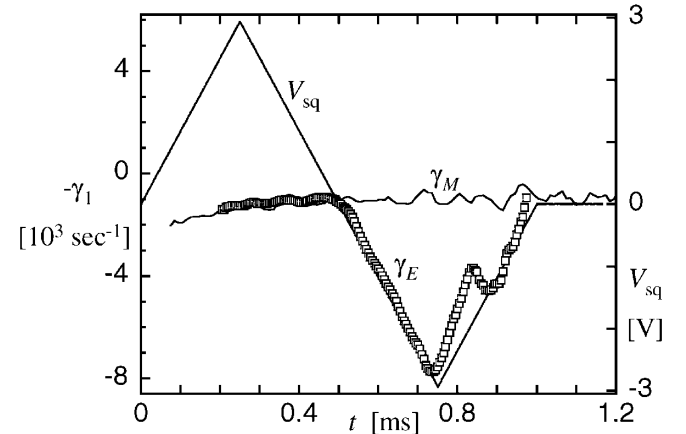


FIG. 5. Enhanced damping γ_E induced by the negative portion of a ramped wall voltage V_{sq} ; the γ_M measurement is for $V_{\text{sq}} = 0$.

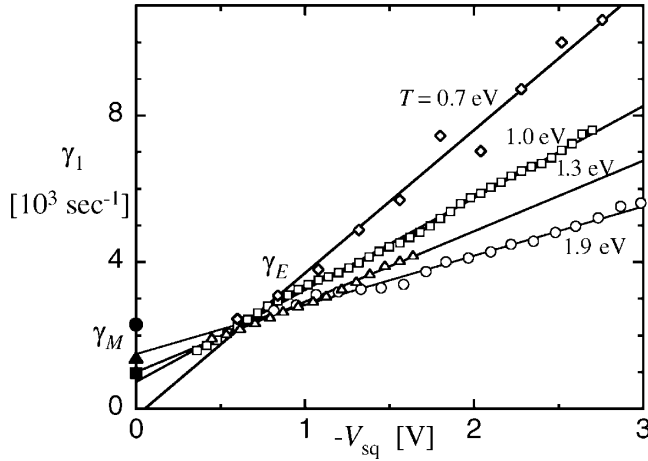


FIG. 6. Damping rate γ_E vs squeeze voltage V_{sq} at various plasma temperatures. Solid symbols show damping rate γ_M at $V_{sq} = 0$.

temperatures are obtained by preheating with end-confinement-voltage variations near the electron bounce frequency of $f_b \sim 1$ MHz.

The temperature dependencies of γ_E and γ_M differ markedly. The observations suggest $\gamma_E \propto eV_{sq}/T$, which probably reflects a dependence on the number of electric-trapped particles, i.e., $\gamma_E \propto N_{tr}/N_{tot}$. This dependence has been observed in prior TPM experiments on damping and transport with electric trapping [3,4]. In contrast, a weakly positive dependence is obtained for $\gamma_M(T)$, but this has not been interpreted theoretically.

This TPM damping shows essentially no dependence on B , verified over the range $1 \leq B \leq 15$ kG where $f_R/f_* \ll 1$. In this regime, the TPM damping rates are essentially equal for the upper and lower BGK modes.

The measured TPM damping rates are approximately $50\times$ larger than a collisional Zakharov-Karpman estimate, which gives $\gamma_{ZK} \sim 20 \text{ sec}^{-1}$. This is consistent with the $80\times$ difference between $\gamma_{ZK} \propto (\nu/f_*)^1 \sim 1.4 \times 10^{-4}$ and the (presumed) $\gamma_{TPM} \propto (\nu/f_*)^{1/2} \sim 1.2 \times 10^{-2}$. However, as yet this $(\nu/f_*)^{1/2}$ scaling of TPM damping has been obtained theoretically only for “trapped-particle diocotron” modes [21], and substantial questions remain as to distribution function discontinuities, dissipation of equilibrium currents, and radial particle transport. Thus, the coefficient remains uncertain.

Of course, this TPM damping of $m_\theta \neq 0$ modes couples wave angular momentum into the plasma particles and causes radial transport of particles. Thus, TPM effects may contribute to the “rotating wall” technique for plasma manipulation and steady-state confinement, in at least some of the regimes where it has been applied [22,23].

In conclusion, these experiments demonstrate that weak ripples in magnetic or electric confinement fields can produce dominant damping effects for nonaxisymmetric

plasma waves. These trapped-particle-mediated damping effects are particularly important in large-amplitude BGK states, where conventional collisional damping is much weaker.

This work was supported by National Science Foundation Grant No. PHY0354979.

-
- [1] A. A. Kabantsev, C. F. Driscoll, T. J. Hilsabeck, T. M. O’Neil, and J. H. Yu, Phys. Rev. Lett. **87**, 225002 (2001).
 - [2] C. F. Driscoll, A. A. Kabantsev, T. J. Hilsabeck, and T. M. O’Neil, in *Non-Neutral Plasma Physics V*, edited by M. Schauer *et al.*, AIP Conf. Proc. No. 692 (AIP, New York, 2003), p. 3; A. A. Kabantsev and C. F. Driscoll, Bull. Am. Phys. Soc. **49**, 318 (2004).
 - [3] A. A. Kabantsev and C. F. Driscoll, Phys. Rev. Lett. **89**, 245001 (2002).
 - [4] A. A. Kabantsev, J. H. Yu, R. B. Lynch, and C. F. Driscoll, Phys. Plasmas **10**, 1628 (2003).
 - [5] M. N. Rosenbluth, D. W. Ross, and D. P. Kostomarov, Nucl. Fusion **12**, 3 (1972).
 - [6] J. Slough, G. A. Navratil, and A. K. Sen, Phys. Rev. Lett. **47**, 1057 (1981).
 - [7] G. A. Navratil, A. K. Sen, and J. Slough, Phys. Fluids **26**, 1044 (1983).
 - [8] H. R. Wilson, J. W. Connor, R. J. Hastie, and C. C. Hegna, Phys. Plasmas **3**, 248 (1996).
 - [9] H. Biglari, P. H. Diamond, and P. W. Terry, Phys. Fluids B **2**, 1 (1990).
 - [10] C. D. Beidler, W. N. G. Hitchon, W. I. van Rij, S. P. Hirshman, and J. L. Shohet, Phys. Rev. Lett. **58**, 1745 (1987).
 - [11] M. Bernstein, J. M. Greene, and M. D. Kruskal, Phys. Rev. **108**, 546 (1957).
 - [12] J. R. Danielson, F. Anderegg, and C. F. Driscoll, Phys. Rev. Lett. **92**, 245003 (2004).
 - [13] J. D. Moody and C. F. Driscoll, Phys. Plasmas **2**, 4482 (1995).
 - [14] W. Bertsche and J. Fajans, Phys. Rev. Lett. **91**, 265003 (2003).
 - [15] V. E. Zakharov and V. I. Karpman, Sov. Phys. JETP **16**, 351 (1963).
 - [16] R. L. Sperling, Phys. Fluids **21**, 514 (1978).
 - [17] I. D. Kaganovich, Phys. Rev. Lett. **82**, 327 (1999).
 - [18] S. A. Prasad and T. M. O’Neil, Phys. Fluids **26**, 665 (1983); A. A. Kabantsev, “TG Mode Frequency Correction,” <http://sdphA2.ucsd.edu>.
 - [19] A. W. Hyatt, C. F. Driscoll, and J. H. Malmberg, Phys. Rev. Lett. **59**, 2975 (1987).
 - [20] A. A. Kabantsev and C. F. Driscoll, Rev. Sci. Instrum. **74**, 1925 (2003).
 - [21] T. J. Hilsabeck, A. A. Kabantsev, C. F. Driscoll, and T. M. O’Neil, Phys. Rev. Lett. **90**, 245002 (2003).
 - [22] F. Anderegg, E. M. Hollmann, and C. F. Driscoll, Phys. Rev. Lett. **81**, 4875 (1998); E. M. Hollmann, F. Anderegg, and C. F. Driscoll, Phys. Plasmas **7**, 1767 (2000).
 - [23] J. R. Danielson and C. M. Surko, Phys. Rev. Lett. **94**, 035001 (2005).